J. Fluid Mech. (1980), *vol.* 101, *part* 1, *pp.* 79–95
Printed in Great Britain

Direct measurements of skin friction in a turbulent boundary layer with a strong adverse pressure gradient

By D. FREI AND H. THOMANN
Institute of Aerodynamics, Swiss Federal Institute of Technology, Zurich

(Received 16 July 1979 and in revised form 19 February 1980)

This paper describes a new balance, suitable for direct measurement of skin friction in turbulent boundary layers with severe pressure gradients. The gaps between the floating element and the surrounding wall are filled with a liquid in order to eliminate disturbing pressure forces on the element. The resulting friction forces are measured with piezo-electric transducers with high sensitivity and extremely small element displacement.

Skin friction measurements were taken in the turbulent boundary layer of a wind tunnel with circular cross-section at $M \leqslant 0{\cdot}25$. Severe adverse pressure gradients were generated by means of a step on the wall or, alternatively, by a conical centre body.

The new apparatus was mainly used to investigate the error of Preston tubes in adverse pressure gradients. It was necessary to develop a new measuring technique to improve the repeatability of the Preston tube readings.

The Preston tube error was found to depend on both the local pressure gradient $P = (dp/dx)\,\nu/\rho u_\tau^3$ and on the Preston tube diameter $u_\tau d/\nu$ and to be independent of the upstream pressure distribution for the range of parameters covered by the experiments.

1. Introduction

The universal 'law of the wall' can be used to determine the skin friction in turbulent boundary layers with small pressure gradients. A well-known method was suggested by Preston (1954) which uses the pressure read by a Pitot tube resting on the wall; Patel (1965) gave limits for the admissible pressure gradients.

For severe pressure gradients, the universal 'law of the wall' is not generally accepted, because it is extremely difficult to measure the skin friction under these conditions. Preston tubes are of little use, as their calibration relies on the 'law of the wall' and floating elements are severely disturbed by the pressure forces acting on the element.

Measuring techniques for the determination of skin friction have been surveyed by Rechenberg (1963) and later by Bertelrud (1972) and Winter (1977). Tomm (1978) gives a description of a laser application for the determination of local skin friction. The measuring tolerances, however, are not yet satisfactory, as the velocity is not measured spotwise but within a finite volume.

A different way to measure skin friction by a direct method could arise from new materials developed in electronics, see Reeder & Cullen (1976). Up to now, however, no publication is known where this technique is used to measure skin friction.

0022-1120/80/4550-2120 $02.00

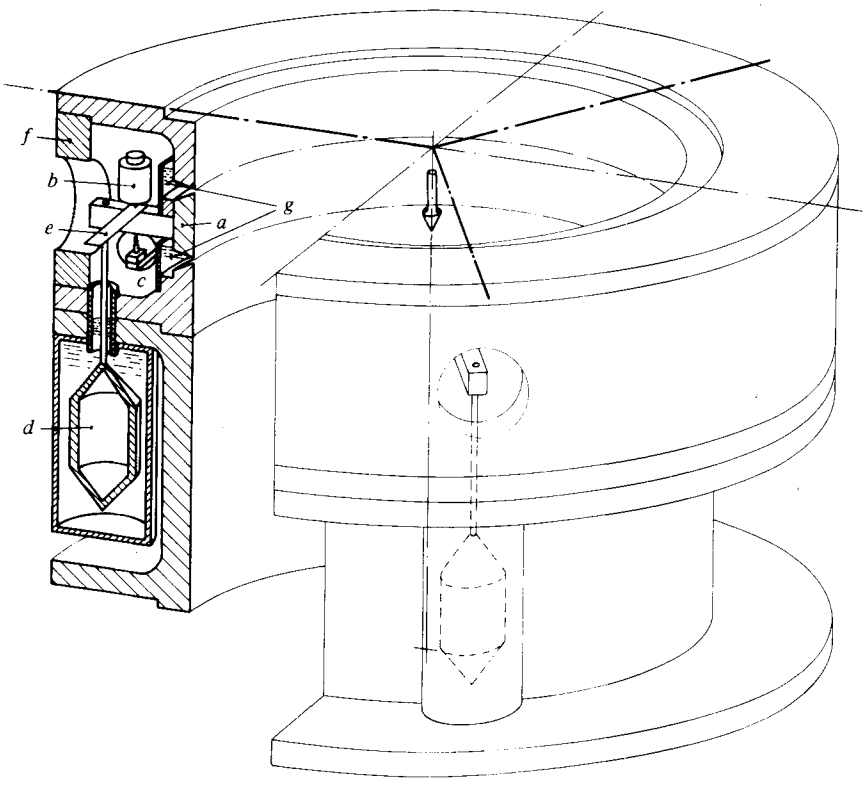

FIGURE 1. Skin friction balance: *a*, floating element (ring); *b*, electro magnet; *c*, force transducer; *d*, float, submerged in oil; *e*, spring leaves; *f*, centre wall; *g*, liquid, sealing the gap.

It was the aim of the present work to determine the skin friction by direct measurement of the force on a floating element and to use these results to calibrate Preston tubes under severe pressure gradients. A new idea is that the surface tension of a liquid can be used to seal the gap. This method will be discussed in detail in the next section. In §§ 3 and 4 the balance and the experimental set-up are described and in § 5 the results are presented.

2. The use of surface tension to seal a floating element

The skin friction balance that has been developed and tested at the Aerodynamical Institute of the Swiss Federal Institute of Technology, Zurich is based on the floating-element principle (see figure 1). The narrow gaps between the surface element and the surrounding walls are filled with a liquid in order to seal them and to eliminate unknown pressure forces on the side walls of the element. The principle is shown in figure 2. For an ideal balance there would be $b_1 = b_2$ and $s_1 = s_2 = 0$. The angle α_1 follows from a force balance in a direction perpendicular to c_1 as

$$\sin \alpha_1 = \frac{p_1 - p_{F1}}{2\sigma} c_1,$$

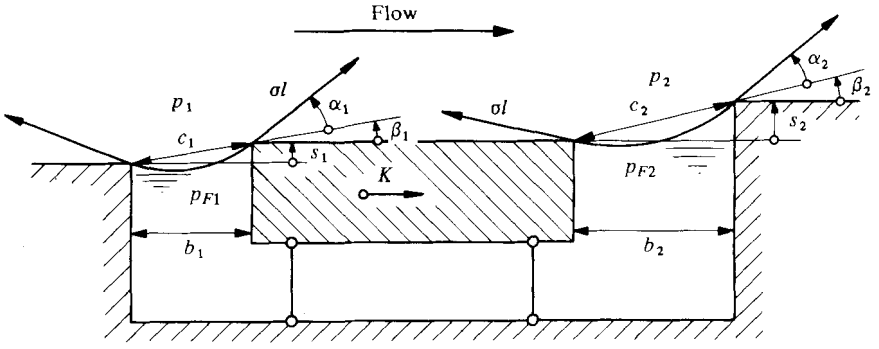

FIGURE 2. Force K acting on a wall element, σ = surface tension, l = length of gap.

where σ is the surface tension of the liquid in the gap. The largest pressure difference that can be supported by the surface tension is found with the condition

$$\sin(\alpha_1+\beta_1) = 1.$$

It is

$$(p_1-p_{F1})_{\max} = \frac{2\sigma b_1}{b_1^2+s_1^2}.$$

For $b_1 = 0{\cdot}1$ mm, $s_1 = 0$ and $\sigma = 7{\cdot}5\times10^{-2}$ N m^{-1} (water) it amounts to 1500 Pa which is considerably more than required by the experiment. Notches in the rim of the element reduce this figure significantly. For $\tau_w = 7$ Pa ($u_e \cong 70$ m s^{-1}) and $p_1-p_{F1} = \pm 200$ Pa the experiments showed a considerable safety margin against loss of fluid.

In spite of slightly lower surface tension, glycerine carried higher loads than water, probably because vibrations are damped more efficiently by the high viscosity. Further reasons for the final choice of glycerine were its low rate of evaporation and the lack of corrosive properties.

Measuring errors caused by surface tension

The skin friction force depends on the surface area of the wall element and the flow condition. In our case, this force may be expected to be less than 0·04 N. The gap length on each side of the wall element will be 628 mm and the gap width $b = 0{\cdot}1$ mm. Error estimates concerning the influence of the surface tension have, therefore, to be based on these conditions.

As shown in figure 2 the tangential force K acting on the element becomes

$$K = \sigma l[\cos(\alpha_2-\beta_2) - \cos(\alpha_1+\beta_1)].$$

From the result for $\sin\alpha$ given above and $\sin\beta = s/c$,

$$\frac{K}{\sigma l} = \frac{b_2}{c_2}\left(1-\left(\frac{p_2-p_{F2}}{2\sigma}c_2\right)^2\right)^{\frac{1}{2}} - \frac{b_1}{c_1}\left(1-\left(\frac{p_1-p_{F1}}{2\sigma}c_1\right)^2\right)^{\frac{1}{2}} + \frac{s_2(p_2-p_{F2})+s_1(p_1-p_{F1})}{2\sigma}.$$

This force will introduce an error if its amount changes between the calibration of the apparatus and the measurement. For the arrangement shown in figure 1 p_{F1} and p_{F2}

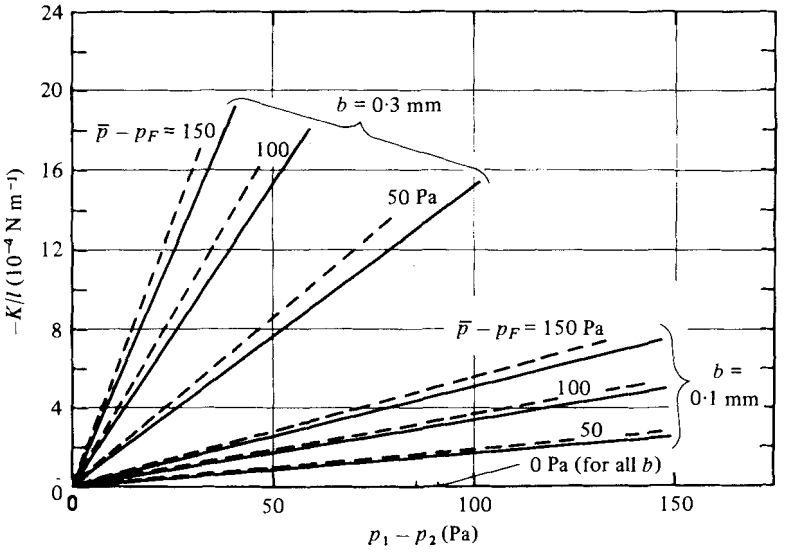

FIGURE 3. Influence of static pressure in the air p_1, p_2 and the liquid p_F on the secondary force K acting on the wall element; $\bar{p} = \frac{1}{2}(p_1+p_2)$, l = length of gap. ——, water ($\sigma = 7{\cdot}5\times10^{-2}$ N m^{-1}); – – –, glycerine ($\sigma = 6{\cdot}7\times10^{-2}$ N m^{-1}).

need not be equal. An indication of the conditions to be satisfied by the balance are found from the following cases.

(*a*) $s_1 = s_2 = 0$, $b_1 = b_2 = b$, $p_{F1} = p_{F2} = p_F$.

The results shown in figure 3 indicate that K becomes small compared with the friction force if the gaps are narrow and if the pressure p_F in the liquid is close to the mean air pressure $\bar{p}$. This second condition was satisfied by venting the space behind the element shown in figure 1 through a static pressure tap located close to the downstream end of the ring.

(*b*) $s_1 = s_2 = 0$, $b_1 = b-t$, $b_2 = b+t$.

This leads to

$$\frac{K}{\sigma l} = \left(1-\left[\frac{p_2-p_F}{2\sigma}(b+t)\right]^2\right)^{\frac{1}{2}} - \left(1-\left[\frac{p_1-p_F}{2\sigma}(b-t)\right]^2\right)^{\frac{1}{2}}.$$

From this equation the need for a stiff force transducer emerges. For the transducer described in § 3, $t \leqslant 10^{-3}$ mm and the error becomes small.

Furthermore, the initial set-up must guarantee that $b_1 = b_2$ with a high accuracy. This could be checked by closing the venting and the test section in figure 1 at both ends which results in $p_1 = p_2$. If K was independent of this pressure, the balance was correctly adjusted.

(*c*) $s_1 = s_2 = s$, $b_1 = b_2 = b$, $p_1 = p_2 = p$, $p_{F1} = p_{F2} = p_F$.

In this case

$$K = ls(p-p_F).$$

With the venting described in (*a*) this error becomes negligible.

(*d*) $s_2 = -s_1$, $b_1 = b_2 = b$, $p_{F1} = p_{F2} = \frac{1}{2}(p_1+p_2)$.

This leads to

$$K = \tfrac{1}{2}ls(p_1-p_2).$$

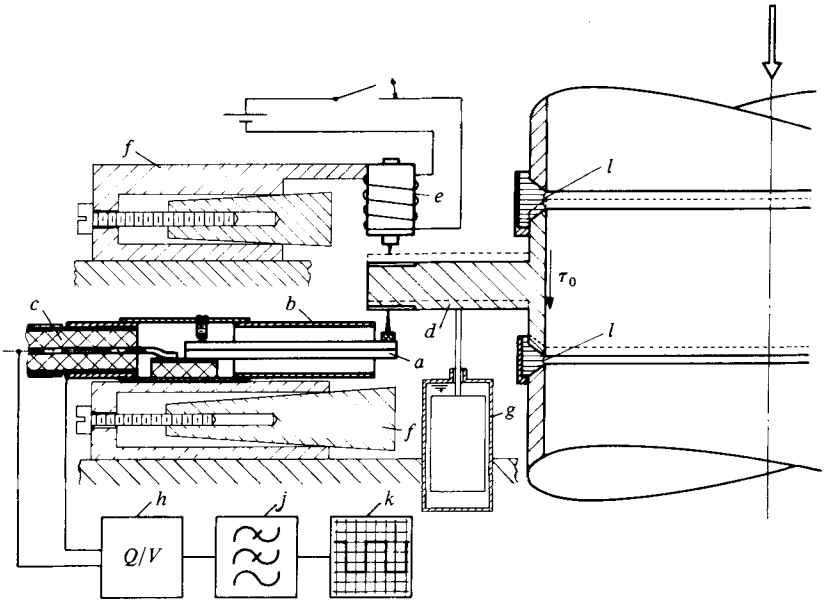

FIGURE 4. Principle of the force measurement: *a*, piezo ceramic bender element, *b*, protecting tube, *c*, HF-cable; *d*, floating element (ring); *e*, electro magnet; *f*, adjusting devices; *g*, floats, submerged in oil; *h*, charge amplifier; *j*, low-pass filter; *k*, display; *l*, gaps, sealed with liquid.

This is the most severe case considered so far. It determines the tolerances for the design of the final balance. Let us give an example: the desired 1 % accuracy of the force measurements results in $K \leqslant 0{\cdot}0004$ N. A maximum pressure gradient in the flow direction may cause a pressure rise of 60 Pa from gap 1 to gap 2. A gap length of 628 mm leads to a maximum allowable misalignment of 0.021 mm. Fortunately it is not very difficult to satisfy this requirement.

3. The skin friction balance

As a detailed description is given by Frei (1979), a few remarks are sufficient here. The experiments were carried out in a vertical tube of 200 mm inner diameter. The hydraulically smooth surface element had the shape of a ring placed between two adjacent tube segments. It was supported by three balances (see figure 4). The bottom stop (*f* in figure 4) adjusts the correct width of the lower gap to 0·1 mm while the upper one limits the movement of the wall element. The width of the wall element between the two gaps is 10 mm. With increasing element width the friction forces to be measured increase. This leads to a better resolution of the wall shear stress. On the other hand, the local resolution of the skin friction gets worse due to the integration over a larger surface area. The error $\Delta\tau_w$ due to the finite-element dimension b in the flow direction is found by expressing $\tau_w(x)$ in a Taylor series. The result is

$$\Delta\tau_w = \frac{1}{b}\int_{x_m-\frac{1}{2}b}^{x_m+\frac{1}{2}b} \tau_w(x)\,dx - \tau_w(x_m) = \frac{d^2\tau_w}{dx^2}\frac{b^2}{24} + O(b^4),$$

with $b = 10$ mm a relative error $\Delta\tau/\tau_w \leqslant 2 \times 10^{-3}$ is found for the step, and the errors

are still smaller for the centre body. A 10 mm element was finally chosen. Some tests with a 30 mm element confirmed these ideas.

Three spring leaves mounted tangentially to the ring in a plane normal to the axis enable the ring to move freely in the axial direction and prevent its radial movement. Owing to the narrow gaps (0·1 mm) between the surface element and the surrounding wall, a force measurement system with small element displacement was required. Piezo-electric bender elements, called 'multimorphs' (Philips 1976), are well suited. The characteristics of such a bender element is virtually independent of temperature, and it is linear within a major part of its range.

The deflexion of a 7 mm-cantilever bender element under a load of 0·01 N is $4{\cdot}4 \times 10^{-4}$ mm. It is well known that the output of such a piezo-electric transducer has a tendency to drift under static conditions. For this reason, the force transducer was periodically unloaded by lifting the element with an electro-magnet. The difference of the output signal between the loaded and the unloaded condition corresponds to the skin friction force plus the weight of the wall element. This latter was made very small by supporting the wall element with floats submerged in oil.

4. Experimental set-up and measuring technique

The test section of the circular wind tunnel with 200 mm internal diameter had a length of 570 mm. The maximum velocity was 80 m s^{-1}. The inlet was described in detail by Pozzorini (1976). The positive pressure gradient was applied by means of either a centre body or a step on the wall. These are shown in figures 7 and 8. A certain disadvantage of the step lies in the fact that the static pressure normal to the wall is not exactly constant. A large part of the centre body was covered with porous areas through which air was sucked to prevent flow separation. The reference velocity u_D was determined with Bernoulli's equation from the pressure difference in the inlet and the area ratio.

It was convenient to keep the balance in a fixed position and to move the centre body or the step in the axial direction. The pressure gradient was determined by measuring two static wall pressures, a distance $\Delta x = 10$ mm apart. Preston tube readings usually show a considerable scatter due to variations of the skin friction normal to the flow direction. Therefore, they had to be integrated along the circumference of the test section to give values that could be compared with the results of the balance. The integration was done by adding 36 readings taken at 10° intervals. By taking 72 readings on several occasions, and using the odd ones in one group and the even ones in a second group, it could be shown that this method of integration did not introduce scatter of more than 0·5 %. Velocities $u(y)$ were determined using

$$u = (2(p_0 - p_w)/\rho)^{\frac{1}{2}},$$

where p_0 is the pressure determined with a Pitot tube (same geometry as Preston tube) and p_w is the static pressure at the wall. No correction for turbulence was made. The distance y from the wall was defined as $y_0 + 0{\cdot}15\,d$ where y_0 is the distance of the tube centre-line from the wall and d is the tube diameter.

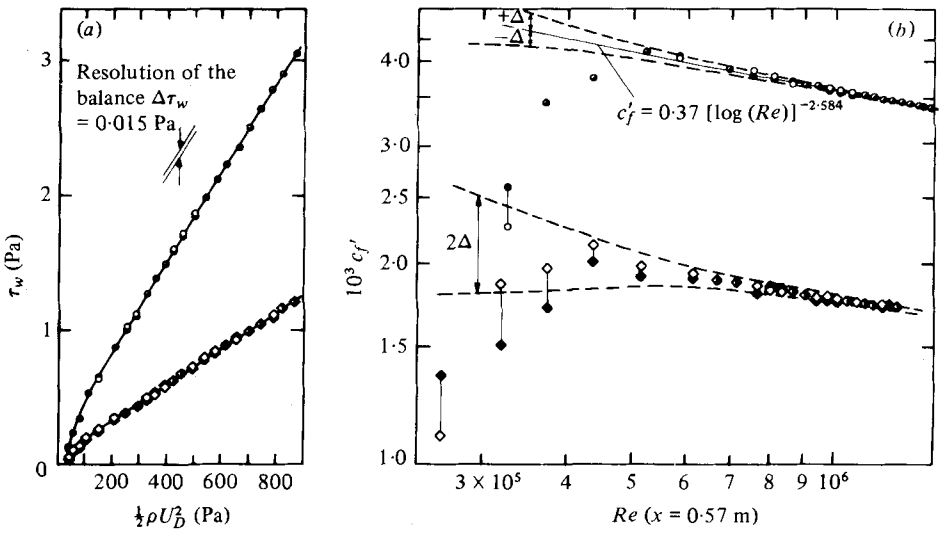

FIGURE 5. Skin friction balance results for variable dynamic pressure, Δ corresponds to the resolution of the balance; ○, ●, $dp/dx \approx 0$; ◇, ◆, $x = 30$ (dp/dx large). The solid line in (*b*) comes from (Schultz-Grunow).

5. Results

Verification of existing results, no pressure gradient

An initial attempt was made to verify the well-known friction law by Schultz-Grunow (1940). The result is given in figure 5. From the comparison between the measurements taken in increasing and decreasing dynamic pressure, one gets a good idea of the repeatability of the skin friction measurements. The measurements were taken in a nominally zero pressure gradient as well as in the area of rising static pressure at 30 mm distance from the step. The zero pressure gradient measurements show excellent agreement with the law by Schultz-Grunow within the indicated measuring tolerances. The deviations at low Reynolds numbers are a consequence of the occurrence of laminar zones.

Figure 6 shows a comparison with Patel's (1965) calibration curve: y^* was determined from τ_w measured with the balance in zero pressure gradient and Δp, averaged as described above, was used in x^*.

Results with strong pressure gradient

Figure 7 shows results for the configuration with the centre body. The pressure distribution, being fairly independent of Reynolds number, is shown for one dynamic pressure only. The skin friction, measured with the balance, is given for four different values of the dynamic pressure. No separation ($\tau_w < 0$) was observed with this configuration. Figure 8 shows comparable results for the step. In this case, negative τ_w were measured 5 to 10 mm in front of the step, clearly indicating flow separation.

Velocity profiles are shown in figures 9 to 11. In figure 9 the friction velocity is $\bar{u}_\tau = (\tau_w/\rho)^{\frac{1}{2}}$ where τ_w was determined with the balance. The agreement with the 'law of the wall' is not convincing. This can be caused either by the pressure gradient or by differences between the local u_τ and $\bar{u}_\tau$. As the boundary-layer probe had the

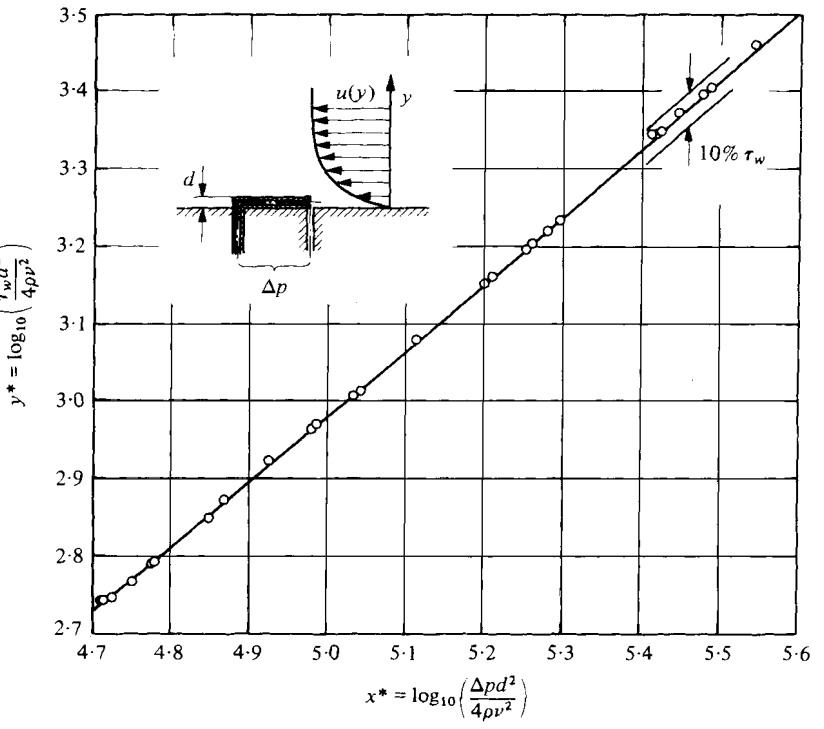

FIGURE 6. Part of Patel's (1965) calibration curve for Preston tubes (——) compared with own measurements (○).

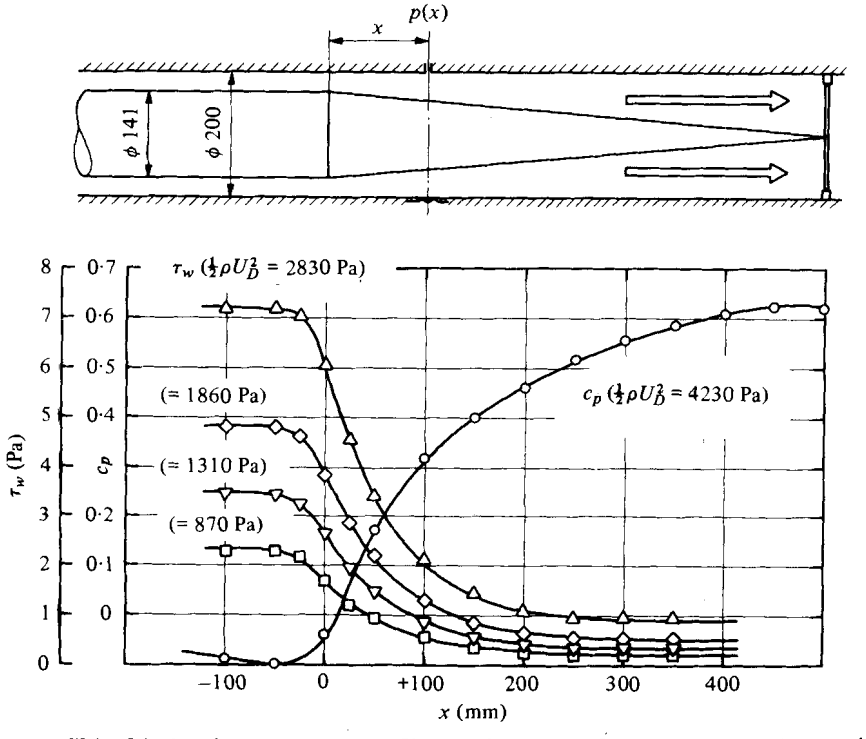

FIGURE 7. Skin friction in a pressure gradient, with centre body; $c_p = 2(p(x)-p_D)/\rho u_D^2$, $p(x)$ is the pressure in the plane of the balance with the centre body displaced by a distance x.

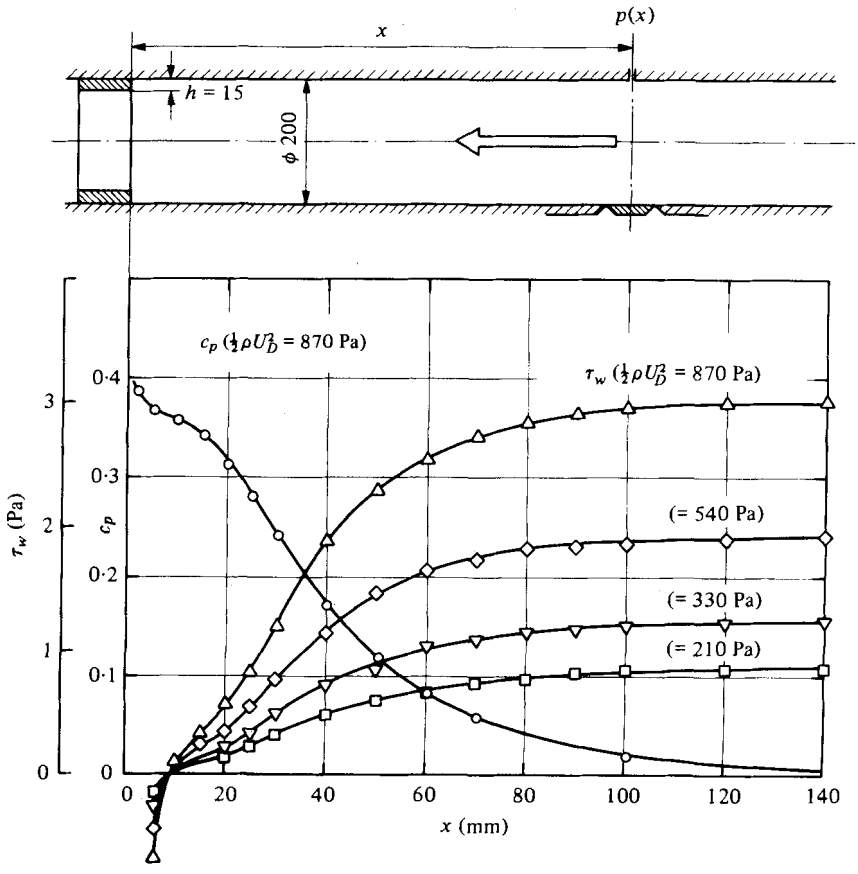

FIGURE 8. Skin friction in front of a step.

same geometry as a Preston tube, the local u_τ could be determined with the reading of the probe resting on the wall and Patel's calibration curve, combined with the corrections given in figure 13. The resulting figure 10 clearly supports the 'law of the wall'. Results for the step are shown in figure 11. They are less reliable, as the pressure gradient normal to the wall was by no means negligible at $x = 30$ mm.

Calibration of the Preston probe in a strong pressure gradient

Preston (1954) showed that a universal relation between τ_w and the pressure Δp read by a Pitot tube resting on the wall can be found if a layer exists close to the wall which depends on *local* parameters only. The thickness of the layer must, of course, be larger than the diameter d of the tube used. For constant pressure, the parameters are τ_w, ρ and ν and dimensional arguments lead to Preston's original relation

$$\frac{\tau_w d^2}{4\rho\nu^2} = \text{fn}\left(\frac{\Delta p\, d^2}{4\rho\nu^2}\right), \tag{1}$$

If the pressure $p(x)$ varies along the wall, the whole upstream history will influence the flow at a station x_1. As $p(x)$ can be expressed as a Taylor series, the upstream history, and thus the flow at x_1, are determined by $dp/dx(x_1)$ and all higher derivatives.

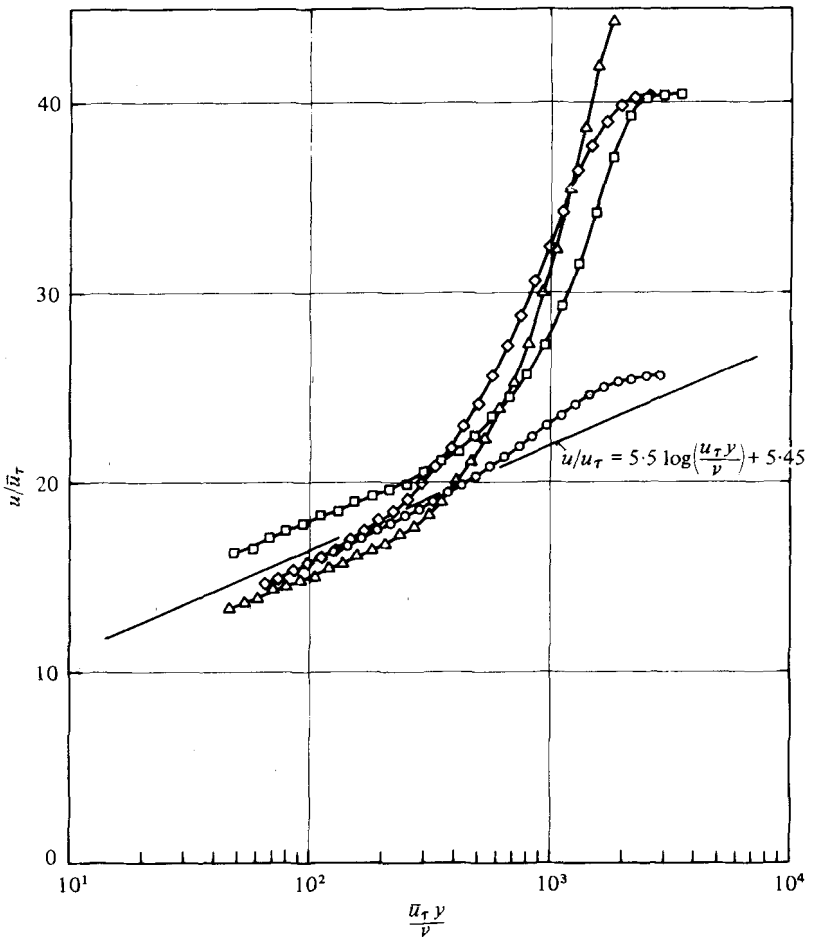

FIGURE 9. Velocity profiles with centre body, $\bar{u}_\tau$ from τ_w measured with the balance, $\frac{1}{2}\rho u_D^2 = 3795$ Pa. ○, $x = -150$ mm, $P = -0{\cdot}001$; ◇, $x = 100$ mm, $P = 0{\cdot}023$; △, $x = 300$ mm, $P = 0{\cdot}016$; □, $x = 450$ mm, $P = 0{\cdot}003$.

Dimensional arguments lead to the following extension of Preston's original relation

$$\frac{\tau_w d^2}{4\rho\nu^2} = \text{fn}\left(\frac{\Delta p\, d^2}{4\rho\nu^2}, P, P', \ldots \frac{u_\tau x_1}{\nu}\right),$$

with

$$P = \frac{dp}{dx}\frac{\nu}{\rho u_\tau^3}, \quad P' = \frac{d^2p}{dx^2}\frac{\nu^2}{\rho u_\tau^4}, \quad \text{etc.}$$

A length scale equivalent, in principle, to x_1 is the local momentum thickness

$$\theta(x_1) = \int_0^\delta \frac{u(x_1, y)}{u(x_1, \delta)}\left[1 - \frac{u(x_1, y)}{u(x_1, \delta)}\right] dy.$$

For a flat plate the universal law of the wall is valid to a distance of about 2θ from the wall and fairly independent of the Reynolds number. Common to almost all data presented by Coles & Hirst (1968) is the fact that this distance decreases to

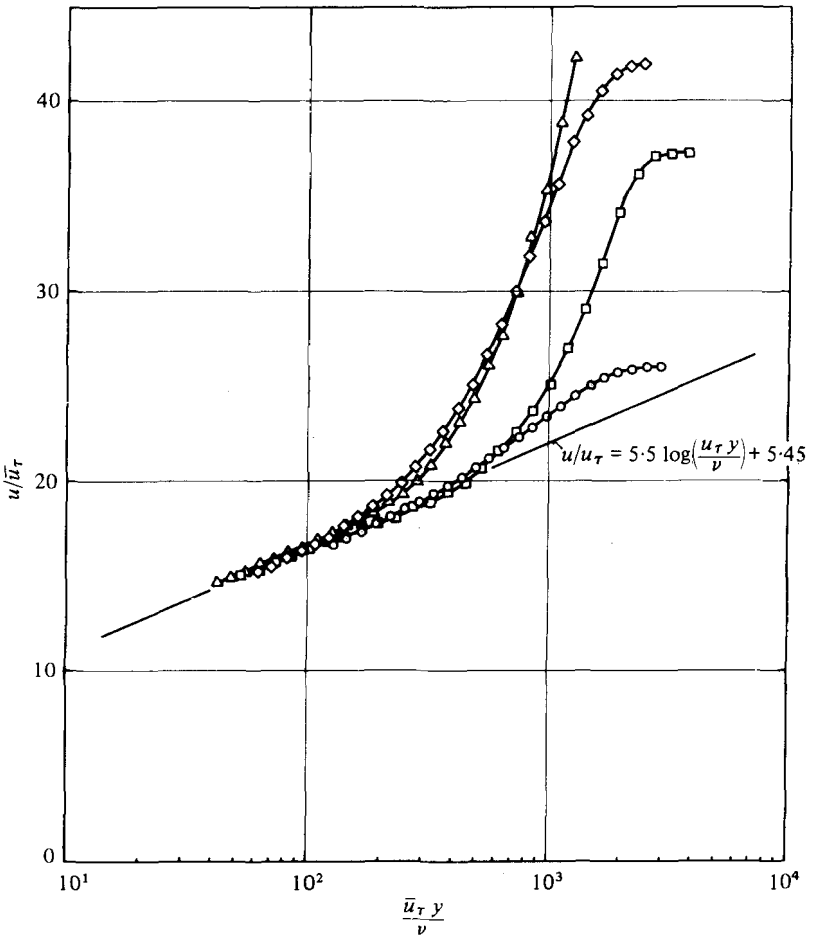

FIGURE 10. Velocity profile with centre body, u_τ from local τ_w determined with the Preston tube. For an explanation of the symbols see figure 9.

about θ for flows approaching separation. θ seems therefore to be a more useful length than x_1. Combining $u_\tau\theta/\nu$ with $u_\tau d/\nu$ results in the parameter θ/d which is suggested to replace $u_\tau x_1/\nu$, leading to

$$\frac{\tau_w d^2}{4\rho\nu^2} = \text{fn}\left(\frac{\Delta p d^2}{4\rho\nu^2},\quad P, P', \ldots,\quad \frac{\theta}{d}\right). \tag{2}$$

The relation $\tau_w = \tau_w(\Delta p)$ should be independent of θ/d as long as the Preston tube is fully submerged in the universal wall layer ($\theta/d = 0{\cdot}5$) for a flat plate). The same can be expected for the flow with a pressure gradient. The limit of $\theta/$d must be determined with the experiment. In our own experiments, tubes with $d = 0{\cdot}5$, 1, 2, 3 and 4 mm and a diameter ratio of 0·6 were used. The resulting θ/d ranged from 1 to 10 for the centre body and from 0·5 to 5 for the step. No systematic dependence of the results on $\theta/$d was found. Further investigations are required to determine a reliable lower limit for θ/d.

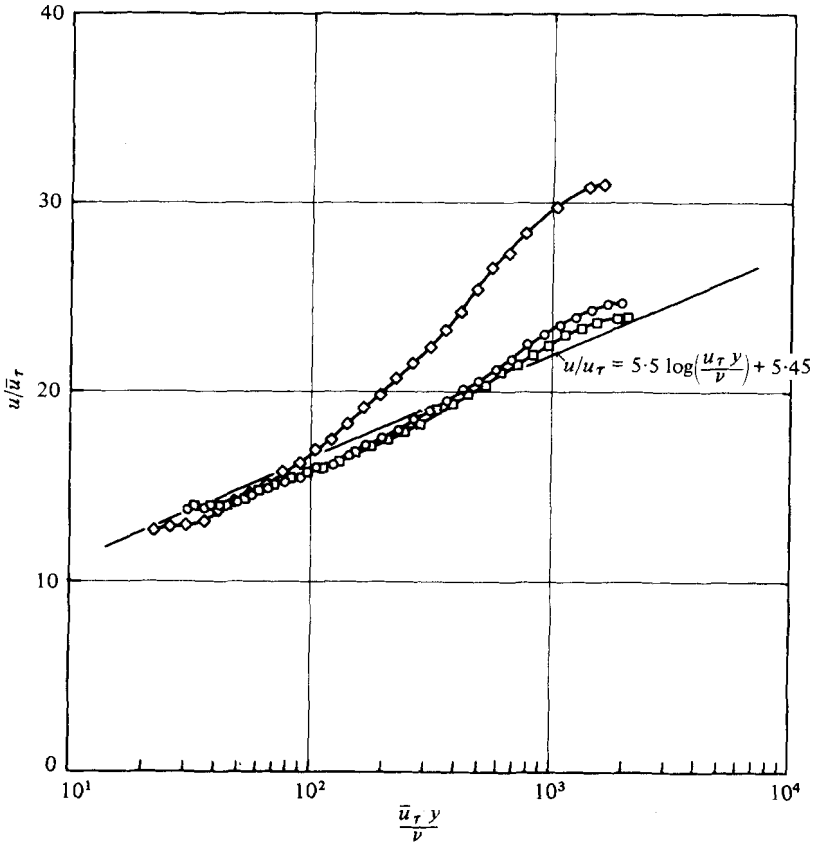

FIGURE 11. Velocity profiles in front of step, $\frac{1}{2}\rho u_D^2 = 850$ Pa. □, $x = 400$ mm, $P = 0{\cdot}000$; ○, $x = 70$ mm, $P = 0{\cdot}0065$; ◇, $x = 30$ mm, $P = 0{\cdot}083$.

Equation (2) is hardly of any use because of the large number of parameters. The first term in a Taylor series usually has the strongest influence. The following simplified form of (2) is therefore suggested

$$\frac{\tau_w d^2}{4\rho\nu^2} = \text{fn}\left(\frac{\Delta p\, d^2}{4\rho\nu^2}, P\right). \tag{3}$$

The results of the present investigation are given in the form

$$\frac{\tau_p - \tau_w}{\tau_w} = \text{fn}\left(\frac{u_\tau d}{\nu}, P\right) \tag{4}$$

which is consistent with (3). The pressure difference Δp, measured with the Preston tube, was averaged as described in §4 and used to determine the apparent, averaged skin friction τ_p with Patel's (1965) original calibration curve; τ_w is the skin friction measured with the balance, a figure averaged over the same circumference. The results are given in figure 12 and tables 1 and 2.

It was suggested by Brown & Joubert (1969) that the Preston tube error should depend on the product of the two parameters, that is

$$\frac{\tau_p - \tau_w}{\tau_w} = \text{fn}\,(P \times u_\tau d/\nu). \tag{5}$$

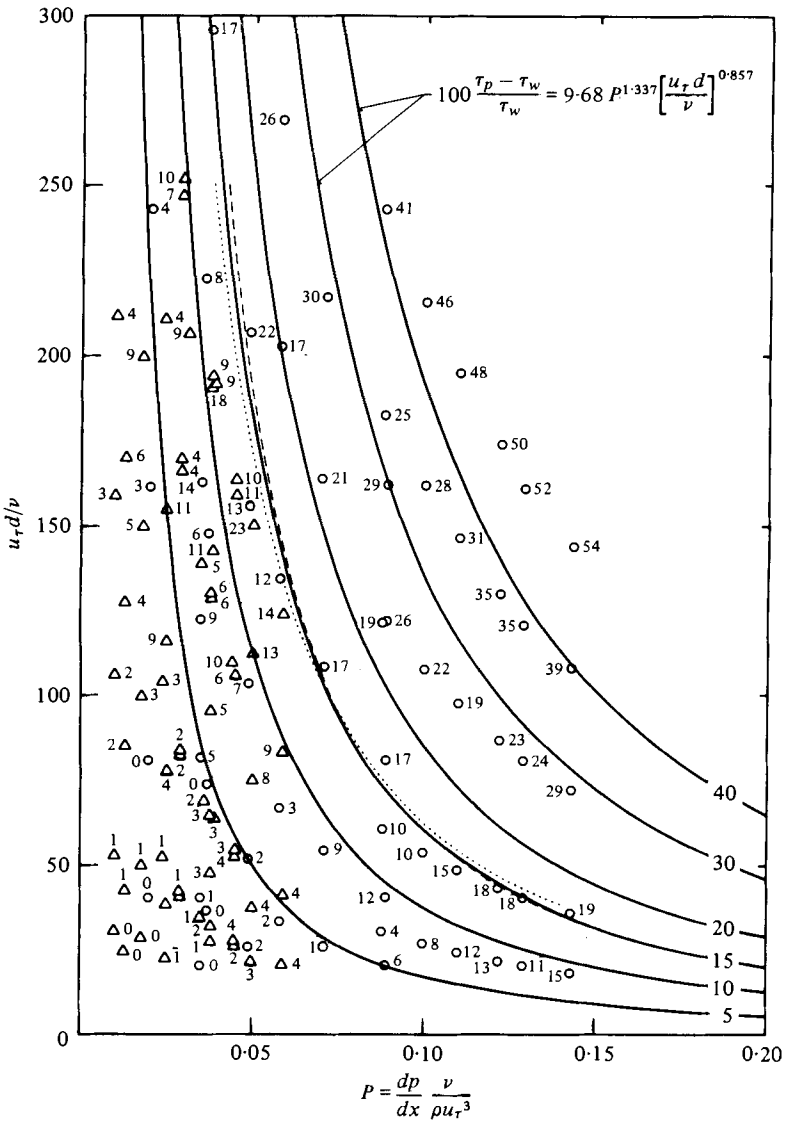

FIGURE 12. Corrections of Preston tube calibration: τ_p = apparent skin friction, determined with Patel's (1965) calibration curve; τ_w = true skin friction, determined with the balance, $u_\tau = (\tau_w/\rho)^{\frac{1}{2}}$. The estimated error in $(\tau_p-\tau_w)/\tau_w$ equals $\pm 0{\cdot}05$ for the least accurate data points and $\pm 0{\cdot}02$ for the most accurate ones. ——, step and centre body: ○, – – –, in front of step; △, ... , with centre body.

If this was true, the curves for constant error shown in figure 12 should be hyperbolas, which is not quite the case. Equation (5) suggests that the following relation might be a reasonable fit to the data:

$$100\frac{\tau_p-\tau_w}{\tau_w}=AP^m\left(\frac{u_\tau d}{\nu}\right)^n. \tag{6}$$

A least-square method was used to determine A, m and n from the data given in tables 1 and 2. The values are

$$A=9{\cdot}68,\quad m=1{\cdot}337,\quad n=0{\cdot}857.$$

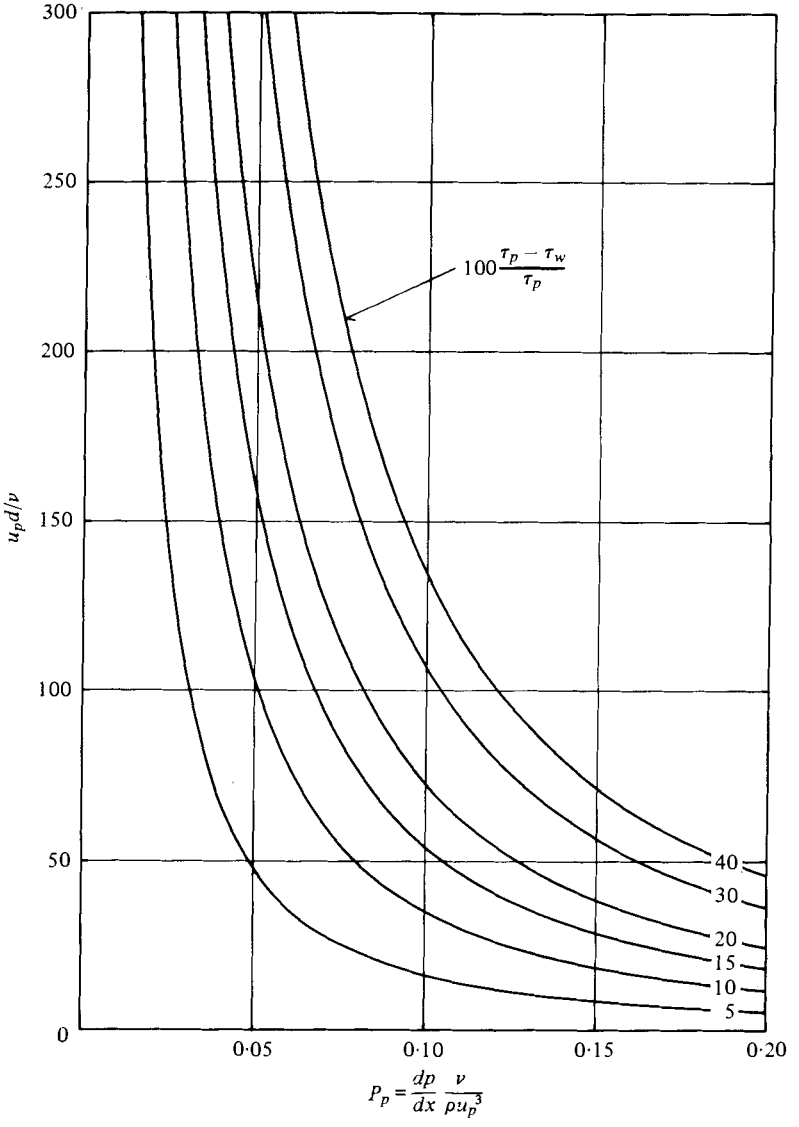

FIGURE 13. Corrections of Preston tube calibration, $u_p = (\tau_p/\rho)^{\frac{1}{2}}$.

Equation (6) was also fitted to the data measured in front of the step (table 1) and, independently, to the data of the centre body (table 2). The two curves for 15 % error in figure 12 show that both arrangements lead to similar results in spite of the different pressure distributions $p(x)$.

Figure 12 and (6) cannot be used directly to reduce experimental data as τ_p is measured and τ_w, P and u_τ are still unknown. In figure 13 the relation

$$100\frac{\tau_p - \tau_w}{\tau_p} = \text{fn}\left(\frac{u_p d}{\nu}, P_p\right) \tag{7}$$

determined from (6) is plotted with

$$u_p = (\tau_p/\rho)^{\frac{1}{2}} \quad \text{and} \quad P_p = \frac{dp}{dx}\frac{\nu}{\rho u_\rho^3}.$$

P	$u_\tau d/\nu$	z	P	$u_\tau d/\nu$	z
0·143	18·0	15·2	0·089	80·8	17·0
0·129	20·1	11·3	0·071	108·4	16·6
0·122	21·6	12·9	0·058	134·2	11·6
0·110	24·3	12·1	0·049	103·2	7·0
0·100	26·9	8·1	0·037	147·4	5·8
0·088	30·3	3·8	0·035	81·1	4·8
0·089	20·2	5·6	0·020	161·0	2·6
0·071	27·1	0·6	0·143	107·9	39·5
0·058	33·5	2·0	0·129	120·5	35·1
0·049	25·8	2·0	0·122	129·9	34·7
0·037	36·8	−0·1	0·110	146·1	31·1
0·035	20·3	0·1	0·100	161·5	28·3
0·020	40·2	0·0	0·088	182.0	24·9
0·143	35·8	19·0	0·089	121·8	26·2
0·129	40·1	18·2	0·070	163·5	21·1
0·122	43·2	17·7	0·058	202·3	17·5
0·110	48·6	14·8	0·049	155·6	13·5
0·100	53·7	9·7	0·036	222·3	8·4
0·088	60·5	9·6	0·035	122·2	9·2
0·089	40·3	12·2	0·020	242·7	3·9
0·071	54·1	9·3	0·143	143·8	54·5
0·058	66·9	3·0	0·129	160·7	51·6
0·049	51·5	2·2	0·122	173·3	50·3
0·037	73·5	0·0	0·110	194·9	48·3
0·035	40·4	1·1	0·100	215·4	46·1
0·020	80·3	−0·5	0·088	242·7	41·3
0·143	71·9	29·2	0·089	161·6	42·0
0·129	80·4	24·4	0·071	217·0	30·3
0·122	86·7	23·2	0·058	268·5	25·6
0·110	97·5	19·0	0·049	206·5	21·6
0·100	107·7	21·7	0·037	295·0	17·3
0·088	121·4	19·2	0·035	162·2	14·0
			0·020	322·1	11·2

TABLE 1. Corrections of Preston tube calibration, in front of step;

$$z = 100\frac{\tau_p - \tau_w}{\tau_w}, \quad P = \frac{dp}{dx}\frac{\nu}{\rho u_\tau^3}.$$

6. Conclusions

The results shown in figure 12 indicate that an equation of the form

$$\frac{\tau_w d^2}{4\rho\nu^2} = \text{fn}\left(\frac{\Delta p\, d^2}{4\rho\nu^2}, P\right) \tag{3}$$

is a good approximation to reality. The next higher parameter in (2) ($P' \sim d^2p/dx^2$) has a range of $0{\cdot}1 \times 10^{-5}$ to 2×10^{-5} for the centre body and 1×10^{-5} to 5×10^{-5} for the step. In spite of this, no significant difference between the two sets of data were found.

Equation (3) implies that the flow in a layer of thickness $O(d)$ depends on local parameters only. If this is true, a law of the wall for the velocity should exist of the form

$$\frac{u}{u_\tau} = \text{fn}\left(\frac{u_\tau y}{\nu}, P\right). \tag{8}$$

P	$u_\tau d/\nu$	z	P	$u_\tau d/\nu$	z
0·024	52·2	1·3	0·029	165·9	4·5
0·029	42·0	1·2	0·038	129·7	5·6
0·035	34·5	1·5	0·045	105·9	6·4
0·038	32·0	2·0	0·059	83·0	8·7
0·045	27·2	4·4	0·038	95·2	5·4
0·029	41·2	0·7	0·050	74·9	7·6
0·038	32·2	2·0	0·010	105·6	1·7
0·045	26·3	1·9	0·013	84·7	2·2
0·059	20·6	4·1	0·018	99·7	3·3
0·038	27·4	1·3	0·025	77·3	4·3
0·050	21·6	2·9	0·029	251·5	10·5
0·010	30·4	0·0	0·031	206·3	8·6
0·013	24·4	0·5	0·039	191·4	9·5
0·018	28·7	−0·4	0·045	163·0	9·8
0·025	22·2	0·8	0·029	246·8	7·4
0·024	104·0	2·6	0·038	193·7	9·5
0·029	83·6	2·2	0·045	158·2	11·0
0·036	68·6	2·3	0·059	123·9	14·1
0·039	63·7	2·9	0·038	142·8	11·2
0·045	54·2	3·5	0·050	112·4	13·5
0·029	82·1	2·4	0·010	158·4	3·0
0·038	64·2	3·1	0·013	127·1	4·1
0·045	52·4	3·9	0·018	149·6	5·4
0·059	41·1	4·5	0·025	115·9	8·9
0·038	47·6	3·1	0·038	190·5	18·1
0·050	37·5	3·9	0·050	149·9	23·2
0·010	52·8	1·2	0·010	211·2	4·4
0·013	42·4	1·4	0·013	169·5	6·3
0·018	49·9	1·4	0·018	199·5	8·8
0·025	38·6	2·5	0·025	154·6	11·1
0·024	210·2	3·9			
0·029	169·0	4·5			
0·035	138·7	4·7			
0·038	128·7	5·8			
0·044	109·6	10·0			

TABLE 2. Corrections of Preston tube calibration, with centre body.

The velocity profiles shown in figures 10 and 11 support this suggestion, but they can hardly serve as proof. The main reason for this remaining uncertainty lies in the fact that it is very difficult to generate a flow that preserves rotational symmetry when approaching separation. Figure 12 shows considerable errors for $u_\tau d/\nu$ as low as 20 which indicates a deformation of the original law of the wall down towards the edge of the laminar sublayer.

Equations (3) and (8) must be used with care close to a pressure maximum. As $P \sim dp/dx$ vanishes there, the next higher term connected with the Taylor series for $p(x)$ ($P' \sim d^2p/dx^2$) should probably be retained in this case.

REFERENCES

BERTELRUD, A. 1972 Skin friction measurement technique in incompressible turbulent flow, a literature survey. *Aero. Res. Inst., Sweden, Tech. Note* AU-726.

BROWN, K. C. & JOUBERT, P. N. 1969 The measurement of skin friction in turbulent boundary layers with adverse pressure gradients. *J. Fluid Mech.* **35**, 737–757.

COLES, D. E. & HIRST, E. A. 1968 Computation of turbulent boundary layers. 1968 *AFOSR–IFP–Stanford Conf.* vol. II.

FREI, D. 1979 Direkte Wandschubspannungsmessung in der turbulenten Grenzschicht mit positivem Druckgradient. *Diss. ETH Nr.* 6392.

PATEL, V. C. 1965 Calibration of the Preston tube and limitation on its use in pressure gradients. *J. Fluid Mech.* **23**, 185–208.

PHILIPS, 1976 Piezo ceramics, permanent magnet materials. *Philips Data Handbook*, part 4*b*, 37–39.

POZZORINI, R. 1976 Das turbulente Strömungsfeld in einem langen Kreiskegel-Diffusor. *Diss. ETH Nr.* 5646.

PRESTON, J. H. 1954 The determination of turbulent skin friction by means of Pitot tubes. *J. Roy. Aero. Soc.* **58**, 109–121.

RECHENBERG, I. 1963 Messung der turbulenten Wandschubspannung. *Z. Flugwiss.* **11**, 429–438.

REEDER, T. M. & CULLEN, D. E. 1976 Surface-acoustic-wave pressure and temperature sensors. *Proc. I.E.E.E.* **64**, 754–756.

SCHULTZ-GRUNOW, F. 1940 Neues Riebungswiderstandsgesetz für glatte Platten. *Luftfahrtforschung* **17** (8), 239.

TOMM, D. 1978 Bestimmung der stationären und instationären Wandschubspannung mit Laser-Doppler-Anemometrie. *Abhandl. Aerodyn. Inst. TH Aachen* 23.

WINTER, K. G. 1977 An outline of the techniques available for the measuring of skin friction in turbulent boundary layers. *Prog. Aerospace Sci.* **18**, 1–57.